OPAL Physics Note PN-295
14 July 1997

Search for a Massive Di-photon Resonance at $\sqrt{s} = 161 - 172$ GeV

The OPAL Collaboration

Abstract

A search for the resonant production of high mass photon pairs associated with a leptonic or hadronic system has been performed using a total data sample of 20.3 pb^{-1} taken at the centre-of-mass energies 161 GeV and 172 GeV with the OPAL detector at LEP. The observed number of events is consistent with the expected number from Standard Model processes. The observed candidates are combined with search results from $\sqrt{s} \approx M_Z$ to place limits on $B(H^0 \to \gamma\gamma)$ within the Standard Model for Higgs boson masses up to 77 GeV, and on the production cross section of any scalar resonance decaying into di-photons. Upper limits on $B(H^0 \to \gamma\gamma) \times \sigma(e^+e^- \to H^0Z^0)$ of 0.29 - 0.83 pb are obtained over $35 < M_H < 160$ GeV.

This note describes preliminary OPAL results to be submitted to the XVIII International Symposium on Lepton-Photon Interactions, Hamburg, 28 July - 1 August 1997, and to the International Europhysics Conference on High Energy Physics, Jerusalem, 19-26 August 1997.

1 Introduction

This paper describes the search for a massive di-photon resonance produced in e^+e^- collisions at $\sqrt{s}$ near the W^+W^- threshold. The search was based on a total of 10.0 pb^{-1} of data taken at $\sqrt{s} = 161.3$ GeV, 1.0 pb^{-1} taken at $\sqrt{s} = 170.3$ GeV, and 9.3 pb^{-1} taken at $\sqrt{s} = 172.3$ GeV; collectively, these energies are referred to as "LEP-2" in this paper. The $\gamma\gamma q\bar{q}$, $\gamma\gamma\ell^+\ell^-$, and $\gamma\gamma\nu\bar{\nu}$ final states are a potentially rich hunting ground for non-Standard Model processes. In the case of the Standard Model Higgs boson, $H^0 \to \gamma\gamma$ proceeds by means of a vertex loop and is too small for observation at existing accelerators even for a kinematically accessible Higgs boson. For example, for an 80 GeV Higgs, the expected $H^0 \to \gamma\gamma$ branching ratio is 1.0×10^{-3}. However, for anomalous Higgs couplings, the production cross section and/or the branching ratio could be large [1]. There are existing limits from data taken at $\sqrt{s} \approx 91$ GeV ("LEP-1") for the production of a di-photon resonance which couples to the Z^0 [2, 3, 4], and measurements of $\gamma\gamma\nu\bar{\nu}$ at $\sqrt{s} \approx 135$ GeV and at LEP-2 have been published [5].

This paper describes the search for a di-photon resonance produced via the process $e^+e^- \to XY$, $X \to \gamma\gamma, Y \to f\bar{f}$ where $f\bar{f}$ may be quarks, charged leptons, or a neutrino pair. For the hadronic and neutrino channels, no requirement is imposed on the mass recoiling from the di-photon system, hence the search is sensitive to any production of the sort $e^+e^- \to XY$, $X \to \gamma\gamma, Y \to$ hadrons.

For a hypothetical di-photon resonance produced at LEP-2 with $M_{\gamma\gamma} > 20$ GeV, the signature is rather distinct from backgrounds because the photons are so energetic. The most important background arises from initial state radiation leading to doubly radiative returns to the Z^0 ($e^+e^- \to Z^0(\gamma\gamma)_{\rm ISR}$).

2 The OPAL Detector

The OPAL detector is described in detail elsewhere [6]; therefore, only the sub-detectors important for this analysis will be described. The electromagnetic calorimeter (EC) consists of lead-glass blocks 24.6 radiation lengths thick, with each block subtending an angular region of approximately 40×40 mrad^2. The "barrel" section of the electromagnetic calorimeter covers the polar region $|\cos\theta| < 0.82$ and the "endcap" sections extends the coverage of the polar region to include $0.81 < |\cos\theta| < 0.98$; the polar angle θ was defined with respect to the incident electron beam direction. Charged track (CT) reconstruction was achieved using a system of cylindrical tracking detectors contained in a uniform 0.435 T magnetic field. The tracking device central to this analysis was the jet chamber. For the polar angle range $|\cos\theta| < 0.92$, charged tracks are reconstructed with nearly 100% efficiency.

For this analysis, the central jet chamber, endcap and barrel electromagnetic calorimeters were required to be fully operational. The most important detector properties for this analysis were the photon angular and energy resolutions, which yielded a di-photon invariant mass resolution (RMS) approximately equal to $\sigma_{M_{\gamma\gamma}} = (0.42 + 0.02M_{\gamma\gamma})$ GeV for scalar production.

Quality cuts on electromagnetic clusters and the accuracy on the modelling of backgrounds varied in several ranges of the polar angle. The polar angle range $0.82 > |\cos\theta| > 0.81$ is the region of overlap between the barrel and endcap electromagnetic calorimeters; electromagnetic clusters are not as well measured in this region. For $0.8 > |\cos\theta| > 0.7$, material from the jet

chamber pressure vessel degrades photon and electron energy measurement somewhat. Inert material in the polar angle range $|\cos\theta| > 0.9$ is the most difficult to model in the detector simulation, and therefore agreement between Monte Carlo simulations and data is poor in this region.

3 Simulation of Signals and Backgrounds

The background sources were modelled by a number of different Monte Carlo simulation programs. The Standard Model backgrounds from $e^+e^- \to (\gamma/Z)^* \to q\bar{q}$ were simulated using the PYTHIA [7] package with the set of hadronization parameters described in reference [8]. Hadronic 4-fermion processes were modelled using the grc4f [9] and EXCALIBUR [10] event generators [1]. The process $e^+e^- \to \gamma\gamma(\gamma)$ was simulated using the RADCOR generator [11]. The programs BHWIDE [12] and TEEGG [13] were utilized to model the background from Bhabha scattering. The processes $e^+e^- \to \ell^+\ell^-$ with $\ell \equiv \mu, \tau$ were simulated using KORALZ [14]. The KORALZ program was also used to generate events of the type $e^+e^- \to \nu\overline{\nu}\gamma(\gamma)$. Four-fermion processes of the type $e^+e^-\ell^+\ell^-$, where $\ell \equiv e, \mu, \tau$, were modelled using the VERMASEREN [15] and grc4f generators. The background contributions from the process $e^+e^- \to e^+e^-q\bar{q}$ were simulated using PYTHIA.

For the simulation of potential signals, both the HZHA generator [16] and the PYTHIA generator were used to simulate the process of $e^+e^- \to H^0Z^0$ followed by $H^0 \to \gamma\gamma$ for each Z^0 decay channel. For the more general production of scalar/scalar and scalar/vector production, $e^+e^- \to XY \to \gamma\gamma + hadrons$, a mass grid was generated. For each X or Higgs mass, 1000 events were generated.

Both signal and background events were processed using the full OPAL detector simulation [17] except for a subset of the mass grid used in the hadronic channel. In the latter case, a fast simulation of the detector was used. The fast simulation was found to be in agreement with the full simulation within the 5% statistical precision of the comparisons. The detector simulation describes the data well except for the low polar angle region mentioned in the previous section.

4 Event Selection

The philosophy adopted in this analysis was to introduce the minimum number of cuts which allow for a relatively uniform acceptance over the largest possible range of masses. The search was divided into three topologies. The first was a search for a massive di-photon system recoiling off of a hadronic system. The second topology was a search for di-photons produced in association with a Z^0 decaying to charged leptons. The third topology was a search for no detector activity other than a di-photon pair. The exceptionally clean nature of the di-photon final states permitted the use of very loose selection criteria to identify the Z^0 decay products.

Radiative events were distinguished by examining the polar angle distribution of the photons. Photons arising from initial state radiation were close to the beam direction, whereas

[1] The EXCALIBUR and grc4f results were compared within the context of this analysis and found to agree within the statistics.

photons from processes of interest, *i.e.* $H^0 \to \gamma\gamma$, would be distributed nearly isotropically. The background was serious for photon energies below approximately 10 GeV, corresponding to masses below about 20-30 GeV for the center-of-mass energies under consideration.

4.1 Photon Identification

To make the photon selection more robust, cuts were made on the lateral spread and isolation of the electromagnetic clusters. Good clusters were required to have lateral sizes consistent with electromagnetic showers. The number of blocks in the cluster (N_{blk}) and the number of blocks containing 90% of the cluster energy (N_{90}) were required to be less than some maximum values, depending on the polar angle of the cluster. Four fiducial regions of the calorimeter were considered, and the barrel region was divided into two regions because of differing amounts of inert material in these regions. Clusters containing blocks having excessive electronic noise were eliminated. The cluster definition cuts were:

- Barrel region I ($|\cos\theta| < 0.7$): $N_{blk} < 15, N_{90} < 3$;
- Barrel region II ($0.7 < |\cos\theta| < 0.81$): $N_{blk} < 25, N_{90} < 4$;
- Barrel-Endcap overlap ($0.81 < |\cos\theta| < 0.82$): $N_{blk} < 35, N_{90} < 5$;
- Endcap ($0.82 < |\cos\theta| < 0.98$): $N_{blk} < 20, N_{90} < 5$.

Photon candidates were then required to satisfy an isolation requirement which rejected events where the electromagnetic cluster energy included particles from the hadronic system. The energy of additional tracks and clusters in a 15° half-angle cone defined by the photon direction had to be less than 2.0 GeV. The distribution of cone energy, after the multiplicity preselection cuts described in the next section, is shown in Figure 1. The distribution of this variable is also shown for the simulated background events. The EC cluster definition cuts reduced the acceptance for the signal by only about 1%. The cone-energy cut has up to a 10% effect, owing to overlap of the photons with the jets in the events.

The minimum energy for an accepted photon candidate was dependent on the channel under study. For the hadronic final state, at least two photons were required to have $x_\gamma > 0.05$ and at least one with $x_\gamma > 0.10$, where x_γ was defined as $E_\gamma/E_{\rm beam}$. For the leptonic and neutrino channels, two photons were required to have $x_\gamma > 0.10$. Figure 2 shows the distribution for x_γ in data and simulated backgrounds, as well as for a potential Higgs signal, after applying the multiplicity preselection cuts described in the next section.

4.2 Hadronic Channel

The hadronic channel consisted of a $\gamma\gamma$ + *hadrons* final state. Candidates for this topology were initially identified by applying a multiplicity preselection consisting of loose charged track multiplicity and visible energy cuts which were used in the standard hadronic event selection described in reference [18]. The preselection cuts were applied to the following measured quantities:

- $E_{\rm vis}$: sum of CJ track energy (assuming m_π), unassociated EC, and unassociated hadron calorimeter clusters;
- $\vec{p}_{vis}$: vector sum of CJ tracks, unassociated EC clusters, and unassociated hadron calorimeter clusters;
- $E_{\rm cm} \equiv 2 \times E_{\rm beam}$

The multiplicity preselection cuts required the event to have at least 5 charged tracks and $R_{\rm vis} > 0.1$, where $R_{\rm vis} \equiv \frac{E_{vis}}{E_{cm}}$. Additional "precuts" rejected radiative and $e^+e^-f\bar{f}$ events using the quantities $R_{\rm vis}$ and $R_{\rm miss} \equiv \frac{|p_{vis}|}{E_{cm}}$:

- $R_{\rm vis} > 0.6$ and $R_{\rm miss} < (0.5 \times R_{\rm vis} - 0.1)$;
- Sum of the visible momentum along the beam direction: $|\Sigma\ p_z^{vis}| < 0.5 E_{\rm beam}$;
- event had at least 2 electromagnetic clusters with $E > 0.05 \times E_{\rm beam}$.

The distributions of $R_{\rm miss}$ and $R_{\rm vis}$ for simulated signal and backgrounds are shown in Figure 3; the effects of the cuts on data and background simulations are shown in Table 1.

At this point, the background events were almost exclusively from doubly radiative events. As indicated in Table 1, there was a dramatic reduction of the backgrounds from all sources simply when two energetic photons were required in the event. An optimal acceptance for the search topology was obtained by imposing cuts on the scaled photon energy:

- Require at least one photon with $x_\gamma > 0.10$;
- Require at least two photons with $x_\gamma > 0.05$.

Figure 4 shows the distribution of the highest photon energy for events passing the precuts and having at least one photon with $E_\gamma > 10$ GeV. The key difference between the doubly radiative photons and those arising from a massive-particle decay is seen in the polar angle distributions of the photons; this is shown in Figure 5. A cut was therefore imposed to eliminate most of the radiative events:

- $|\cos\theta_{\gamma 1,2}| < 0.9$ and $|\cos\theta_{\gamma 1}| + |\cos\theta_{\gamma 2}| < 1.4$.

After the cuts on θ_γ, the agreement between data and background simulations (Table 1) was good. Four events satisfied all cuts at this point, which can be compared to the Standard Model expectation of 2.6 ± 0.5 events (statistical error). The efficiency for this analysis to accept H^0Z^0 events for $M_H = 40$ and 70 GeV is shown in Table 1. Throughout the mass range of interest, an efficiency greater than 45% was maintained.

4.3 Charged Leptonic Channel

The exceptionally clean nature of the $\gamma\gamma\ell^+\ell^-$ final state obviated requiring well-identified leptons. No separation between the e, μ and τ channels was made; therefore, the analysis maintained a high acceptance for the hadronic τ decays. As in the hadronic channel, the most serious background for this channel was doubly radiative returns to the Z^0. Bhabha scattering with initial and/or final state radiation was also a potential background.

The charged lepton channel analysis differed from the hadronic channel in that the event reconstruction included applying a jet finding algorithm. Isolated electromagnetic calorimeter clusters and charged tracks satisfying the selection criteria described in reference [19] were combined into jets using the Durham recombination scheme [20] evaluated with $y_{cut} = 0.02$. Candidates were required to have at least two jets where the two highest energy electromagnetic clusters satisfying the isolation and cluster quality criteria of Section 4.1 were not included.

To reduce the background from doubly radiative returns, a likelihood selection based on the photon polar angle distributions was utilized. The relative likelihood of the di-photon system to be consistent with $H^0 \to \gamma\gamma$ was defined as:

$$\mathcal{L}(\gamma\gamma) = \frac{L(s)}{L(s) + L(b)},$$

where s and b referred to signal and background respectively, and

$$L(x) = \prod_{i=1,2} P(|\cos\theta_{\gamma_i}|),$$

where $P(|\cos\theta_{\gamma_i}|)$ was the probability of observing photon i at a given $|\cos\theta|$. The reference distributions for the background were taken from $e^+e^- \to f\bar{f}\gamma\gamma$ simulations, where $f \equiv \mu, \tau, \nu$. For the signal distributions, H^0Z^0 production was assumed with Higgs masses ranging from 30 to 80 GeV. The $|\cos\theta|$ distribution exhibited negligible dependence upon the Higgs mass and $\sqrt{s}$.

Leptonic channel candidates were required to satisfy the following basic selection criteria (referred to as $\ell\ell\gamma\gamma$ preselection):

- Low multiplicity pre-selection [21];
- Precuts particular to the leptonic channel:
  - Visible energy fraction: $R_{\rm vis} > 0.2$;
  - Number of EC clusters not associated with tracks: $2 \leq N_{\rm EC} \leq 10$;
  - Number of good charged tracks: $2 \leq N_{\rm CT} \leq 7$;
  - Momentum fraction along the beam direction: $|\Sigma\ p_z^{vis}| < 0.7 E_{\rm beam}$.

The following addtional criteria were then imposed:

- At least two EC clusters having $15° < \theta < 165°$ and $x_\gamma > 0.1$ satisfying the cluster quality of section 4.1;

- At least two jets found (excluding the photon candidates) within the Durham scheme using $y_{cut} = 0.02$;
- Photon likelihood: $\mathcal{L}(\gamma\gamma) > 0.4$;
- Recoil mass consistent with the Z^0 mass: $|M_{recoil} - M_Z| < 20$ GeV, where the recoil mass was computed using the di-photon system.

For events passing the cuts before that on the photon likelihood, the distribution of photon angles is shown in Figure 6. No candidate events were selected at either center-of-mass energies. The contribution from Standard Model processes after the application of all selection criteria was 1.0 ± 0.1 at $\sqrt{s} = 161$ and 172 GeV, where the error is statistical. The analysis is summarized in Table 2, where the expected background from leptonic and $e^+e^-f\bar{f}$ 4-fermion final states is compared to the observed number of events. The acceptance for $H^0 \to \gamma\gamma$ ranged from 43-48% for different Higgs masses.

4.4 Missing Energy Channel

The missing energy channel was characterized by a pair of photons recoiling against a massive, unobserved system. The only Standard Model process expected to contribute was doubly radiative return to the Z^0 followed by $Z^0 \to \nu\bar{\nu}$. Potential physics backgrounds included $e^+e^- \to \gamma\gamma(\gamma)$ and radiative Bhabha scattering with one or more unobserved electrons. Backgrounds due to cosmic rays and beam-wall and beam-gas interactions were dealt with as described in reference [22]. Candidates were then required to satisfy in addition the following basic selection criteria (referred to as $\nu\bar{\nu}\gamma\gamma$ preselection):

- 2 electromagnetic clusters with $x_\gamma > 0.1$, satisfying the cluster quality and isolation criteria described in section 4.1;
- $|\Sigma\ p_z^{vis}| < 0.75 E_{\rm beam}$;
- Sum of the scaled photon energies: $x_{\gamma 1} + x_{\gamma 2} < 1.4$;
- Direction of event missing momentum: $|\cos\theta_{\rm miss}| < 0.96$;
- Charged track veto: events were required to have no charged track candidates with 20 or more jet chamber hits satisfying the charged track selection criteria defined in [19];
- Excess calorimeter energy (E_{excess}): the energy observed in the electromagnetic calorimeter not associated with the 2 photons was required to be less than 3 GeV.

At this point the sample was dominated by Bhabha events at small polar angles. The following additional cuts were applied:

- For each photon polar angle: $15° < \theta < 165°$;
- Photon likelihood: $\mathcal{L}(\gamma\gamma) > 0.4$. The photon candidates were required to pass the likelihood selection described in Section 4.3;

Three candidates were selected by these cuts; this is in reasonable agreement with the Standard Model expectation of 1.2 ± 0.1 events where the error is statistical. The distribution of recoil mass for these events is shown in Figure 7. A summary of the effect of the cuts is given in Table 3 where the efficiencies for Higgs masses of 40 and 70 GeV are also given. The acceptance varied from 42 to 64 % depending on the Higgs mass and center-of-mass energy.

5 LEP-1 Analysis

Earlier searches for the production of a scalar resonance coupling to the Z^0 have been performed using the OPAL detector [2, 3]. For these analyses at $\sqrt{s} \approx 91$ GeV, there is a large backround for di-photon masses below appoximately 40 GeV. A large component of this background arises from decays of isolated π^0 and η mesons, which are difficult to model accurately with the current hadronization generators. Therefore, the LEP-1 and LEP-2 analyses are compared only for $M_{\gamma\gamma} > 40$ GeV.

In reference [3], $\ell^+\ell^-\gamma\gamma$ ($\ell = e, \mu, \tau$) and $\nu\bar{\nu}\gamma\gamma$ final states were investigated. From a data sample consisting of 43 pb^{-1}, corresponding to 1.44 million observable Z^0 decays, 2 candidates with $M_{\gamma\gamma} > 40$ GeV were selected in the $e^+e^-\gamma\gamma$ channel and 2 candidates in the $\mu^+\mu^-\gamma\gamma$ channel. The background expected from the dimuon channel was 1.2 ± 0.3 events.[2]

The hadronic channel was investigated applying the analysis described in Section 4.2 to LEP-1 data from the years 1991 - 1994. A sample of 140 pb^{-1} events was used in this analysis, accumulated at energies between 88.28 and 94.28 GeV, and corresponding to 3.51 million hadronic Z^0 decays [2]. The hadronic channel analysis observed 3 candidates having di-photon mass greater than 40 GeV with an expected background of 5.4 ± 3.0 events.

6 Results

The di-photon invariant mass distribution for the events passing all cuts is shown in Figure 8; the simulation of Standard Model backgrounds is also shown in the figure. Summing over all expected background sources yields 4.8 ± 0.5 events expected versus 7 observed. Moreover, the qualitative agreement between the data and simulation of Standard Model processes is good; therefore no new physics process is suggested. After requiring a minimum di-photon mass of 35 GeV, 4 candidates from the LEP-2 data were left, with the missing-energy and hadronic channels each contributing 2 events; this compares well with the 2.9 ± 0.5 expected from Standard Model backgrounds. The kinematic properties of the candidate events are summarized in Table 4.

The uncertainties pertinent to the limits on production rates and di-photon branching ratios arose from statistics of the data, systematic uncertainty on the luminosity, statistical errors on background simulations, and a systematic error derived from the level of concordance between backgrounds and their simulation. The systematic error on the integrated luminosity of the data, 0.6%, contributed negligibly to the limits. Statistical uncertainty on the predicted Standard Model background was dominated by the PYTHIA sample, for which 3000 pb^{-1} was

[2] An evaluation of the expected background was only available for the muon channel due to the lack of availability of an event generator with multiple hard photons at the time of the analysis.

generated at the LEP-2 energies. After the cuts on θ_γ and E_γ, which effectively removed the 4-fermion and 2-photon backgrounds, the remaining background was modelled very well by PYTHIA, as evidenced in Figures 2 and 4. The systematic uncertainty on the background modelling was assessed by varying the cuts by one standard deviation on the quantity involved. The cuts on photon energies are very robust; uncertainties in electromagnetic cluster energies contribute negligibly to the systematic error. The cut most sensitive to background simulation and detector resolution is that on the photon polar angles. The method of cuts variation gives a possible increase in expected backgrounds smaller that the statistical error on the simulation datasets, approximately 0.5 events in the hadronic channel for the LEP-2 data. The same cut-variation technique applied to the efficiency for an expected signal yields a contribution to the systematic uncertainty which is much smaller than the uncertainty from simulation statistics.

The 161 GeV and 172 GeV data have been combined in order to set limits on the product of the production cross section with the di-photon branching fraction. From the events passing the cuts, the 95% C.L. upper limit (CLUL) on the number of events at a given di-photon mass was computed using the method of Bock [23]. The method, which is similar to those reported in reference [24], introduced for every candidate event a weight based on the di-photon mass resolution; it computed a mass-dependent 95% confidence level upper limit based on the total weight-sum of all candidate events.

The expected backgrounds *were not subtracted* in computing the 95% CLUL which results in conservative upper limits. Furthermore, when the statistical method of Bock is used to present the results, where each candidate event weakens the CLUL only in the vicinity of its mass, very little degradation in the upper limits is seen. The results, in the form of upper limits on production cross section (times di-photon branching fraction) are shown in Figure 9. In computing these limits, the efficiency was set to 0 for recoil masses less than 10 GeV. The step-like nature of the limit between di-photon masses of 90 and 120 GeV is due to the recoil mass cut in the charged lepton channel and the cut on photon energies in the missing energy channel. The step at 151 GeV is due to the increase in kinematic region afforded by the highest energy (172 GeV) data. The limits from LEP-1 are compared to those obtained at LEP-2 energies in Figure 9. The larger LEP-1 event sample affords a better limit in the di-photon mass range below 85 GeV. The LEP-2 events allow for limits up to nearly twice the LEP-1 energy.

The Standard Model H^0Z^0 production cross section can be factored out of the limits given in Figure 9 to set upper limits on the branching fraction for $H^0 \to \gamma\gamma$ within the context of this model. This factorization affords a more meaningful presentation of the LEP-2 data because of the large phase space factors at $\sqrt{s} = 161 - 172$ GeV. The resulting limits on $B(H^0 \to \gamma\gamma)$ are shown in Figure 10, where the limits obtained separately from LEP-1 and LEP-2 are compared. Within the Standard Model, the $H^0 \to \gamma\gamma$ branching fraction is calculated to be on the order of 0.1% (i.e., for $M_H = 80$ GeV). However, anomalous couplings could increase the di-photon branching fraction. Therefore, Figure 10 sets limits on the di-photon branching fraction up to $M_H = 77$ GeV.

More general limits on $e^+e^- \to XY$ production can be obtained using the hadronic channel alone. To compute $M_{\gamma\gamma}$ dependent limits, the PYTHIA and HZHA generators have been used to generate a grid of X and Y (recoil particle) masses. It was assumed that X was a scalar and the cases where Y was a vector or scalar were investigated. The resulting efficiencies were found to be almost equal. Using only the LEP-2 data, limits were computed using the efficiency at a given $M_{\gamma\gamma}$ which was the minimum for variation of M_Y. The limits thus obtained are shown in

Figure 11.

7 Conclusions

Using a data sample of 20.3 pb^{-1} taken at center-of-mass energies 161 and 172 GeV, a search for a massive di-photon resonance has been performed. For $M_{\gamma\gamma} > 35$ GeV, a total of 4 candidates survived all selection requirements. The number of observed candidates was consistent with the Standard Model prediction of 2.9 ± 0.5 background events. Upper limits on $B(H^0 \to \gamma\gamma) \times \sigma(e^+e^- \to H^0Z^0)$ of 0.29 - 0.83 pb are obtained over $35 < M_H < 160$ GeV. From the LEP-2 hadronic channel alone, an upper limit on $B(X \to \gamma\gamma) \times B(Y \to hadrons) \times \sigma(e^+e^- \to XY)$, for X a scalar particle, can be placed at 0.29 pb over the mass range $47 < M_{\gamma\gamma} < 160$ GeV. These results can be interpreted within the context of the Standard Model to set a limit on $B(H^0 \to \gamma\gamma)$ up to a Higgs boson mass of 77 GeV, provided the Higgs particle is produced via $e^+e^- \to H^0Z^0$.

References

[1] K. Hagiwara and M.L. Strong, Z. Phys. **C62** (1994) 99.

[2] OPAL Collab., G. Alexander *et al.*, Z. Phys. **C71** (1996) 1.

[3] OPAL Collab., P. Acton *et al.*, Phys. Lett.311 (1993) 391.

[4] L3 Collab., M. Acciarri *et al.*, Phys. Lett.388 (1996) 409;
Delphi Collab., P.Abreu *et al.*, Z. Phys. **C72** (1996) 179.

[5] OPAL Collab., G. Alexander *et al.*, Phys. Lett. **B376** (1996) 315;
OPAL Collab., K. Ackerstaff *et al.*, Phys. Lett. **B391** (1997) 210.

[6] OPAL Collab., K. Ahmet et al., Nucl. Instrum. Meth. **A305** (1991) 275;
P.P. Allport *et al.*, Nucl. Instrum. Meth. **A324** (1993) 34;
P.P. Allport *et al.*, Nucl. Instrum. Meth. **A346** (1994) 476;
O.Biebel *et al.*, Nucl. Instrum. Meth. **A323** (1992) 169;
M.Hauschild *et al.*, Nucl. Instrum. Meth. **A314** (1992) 74.

[7] PYTHIA 5.721 and JETSET 7.408 generators: T. Sjöstrand, Comp. Phys. Comm. **82** (1994) 74; T. Sjöstrand, LUTP 95-20. "PYTHIA 5.7 and JETSET 7.4, Physics and Manual", CERN-TH. 7112/93.

[8] OPAL Collab., G. Alexander *et al.*, Z. Phys. **C69** (1996) 543.

[9] J. Fujimoto *et al.*, *GRC4F V1.1: A four fermion event generator for* e^+e^- *collisions*, preprint KEK-CP-046 and e-Print Archive: hep-ph/9605312.

[10] F.A. Berends, R. Pittau and R. Kleiss, Comp. Phys. Comm. **85** (1994) 43.

[11] F.A. Berends and R. Kleiss, Nucl. Phys.**B186** (1981) 22.

[12] S. Jadach, W. Placzek and B. F. L. Ward, University of Tennessee preprint, UTHEP 95-1001 (unpublished).

[13] D. Karlen, Nucl. Phys.**B289** (1987) 23.

[14] S. Jadach et al., Comp. Phys. Comm. **66** (1991) 276.

[15] J. A. M. Vermaseren, Nucl. Phys. **B229** (1983) 347.

[16] HZHA generator: P. Janot, in *Physics at LEP2,* edited by G. Altarelli, T. Sjöstrand and F. Zwirner, CERN 96-01, vol.2 (1996) p.309.

[17] J.Allison *et al.*, Nucl. Instrum. Meth. **A305** (1992) 47.

[18] OPAL Collab., G. Alexander *et al.*, Z. Phys. **C52** (1991) 175.

[19] OPAL Collab., G. Alexander *et al.*, Z. Phys. **C72** (1996) 191.

[20] N. Brown and W.J. Stirling, Phys. Lett. **B252** (1990) 657;
S. Bethke, Z. Kunszt, D. Soper and W.J. Stirling, Nucl. Phys. **B370** (1992) 310;
S. Catani *et al.*, Phys. Lett. **B269** (1991) 432;
N. Brown and W.J. Stirling, Z. Phys. **C53** (1992) 629.

[21] OPAL Collab., R. Akers *et al.*, Z. Phys. **C61** (1994) 19.

[22] OPAL Collab., R. Akers *et al.*, Z. Phys. **C65** (1995) 47.

[23] P. Bock, OPAL institute publication IP059, 26 June 1997 (submitted to Nucl. Instrum. Meth.).

[24] E. Gross and P. Yepes, Int. Journ. Mod. Phys. **A**8 (1993) 407;
J.F. Grivaz and F. Le Diberder, Nucl. Instrum. Meth. **A333** (1993) 320;
V. F. Obraztsov, Nucl. Instrum. Meth. **A316** (1992) 388.

Cut	Data	ΣBkgd	$(\gamma/Z)^*$	4f	$e^+e^-q\bar{q}$	H40	H70
161 GeV							
Multiplicity	1525	1429.6	1343.8	55.2	30.6	0.97	0.99
Precuts	523	515.3	484.1	30.7	0.5	0.87	0.93
$N_\gamma \geq 2$	10	5.4	5.3	0.1	0.0	0.55	0.61
$\cos\theta_\gamma$ cut	3	1.9	1.9	0.0	0.0	0.48	0.47
172 GeV							
Multiplicity	1409	1247.9	1093.5	125.6	29.0	0.99	0.99
Precuts	461	445.2	366.4	78.5	0.3	0.87	0.92
$N_\gamma \geq 2$	7	5.2	5.2	0.0	0.0	0.67	0.60
$\cos\theta_\gamma$ cut	1	0.7	0.7	0.0	0.0	0.53	0.48

Table 1: Events remaining in the hadronic channel search after cumulative cuts indicated. The background simulation samples are scaled to 10.0 pb^{-1} for $\sqrt{s} = 161$ GeV, and to 10.3 pb^{-1} for $\sqrt{s} = 172$ GeV. In addition to the total simulated background, the simulations for $(\gamma/Z)^*$, 4-fermion ("4f"), and Two-photon ($e^+e^-q\bar{q}$) states are shown. "H40" and "H70" indicate the efficiency for simulation of H^0Z^0events with the Higgs mass equal to 40 and 70 GeV, respectively.

Cut	Data	ΣBkgd	e^+e^-	$\tau^+\tau^-$	$\mu^+\mu^-$	e^+e^-ff	H40	H70
161 GeV								
$\ell\ell\gamma\gamma$ presel.	434	183.41	72.75	46.80	6.73	57.13	0.77	0.81
$N_\gamma \geq 2$	5	5.28	3.44	0.94	0.80	0.10	0.62	0.67
$N_{\rm jet} \geq 2$	1	3.21	1.70	0.67	0.74	0.10	0.60	0.65
$\mathcal{L}(\gamma\gamma)$	0	1.33	0.61	0.33	0.39	0.00	0.49	0.53
$M_{\rm recoil}$	0	0.60	0.24	0.15	0.21	0.00	0.46	0.48
172 GeV								
$\ell\ell\gamma\gamma$ presel.	323	172.61	67.77	39.92	5.80	59.12	0.77	0.80
$N_\gamma \geq 2$	5	4.70	2.74	0.83	0.69	0.43	0.61	0.60
$N_{\rm jet} \geq 2$	1	2.65	1.08	0.61	0.63	0.33	0.58	0.58
$\mathcal{L}(\gamma\gamma)$	0	1.17	0.42	0.32	0.32	0.10	0.49	0.47
$M_{\rm recoil}$	0	0.36	0.08	0.14	0.15	0.00	0.43	0.45

Table 2: Events remaining after cumulative cuts indicated, for the leptonic channel analysis. The row denoted "$\ell\ell\gamma\gamma$ presel." refers to the combined general low-multiplicity selection and the precuts described in Section 4.3. The contributions from Bhabha scattering, μ-pair, τ-pair production and $e^+e^-f\bar{f}$ final states determined from background simulations are shown. The simulated datasets have been normalized to 10.0 pb^{-1} for $\sqrt{s} = 161$ GeV, and to 10.3 pb^{-1} for $\sqrt{s} = 172$ GeV. Also shown is the acceptance for a Higgs signal for 40 and 70 GeV mass denoted as columns "H40" and "H70", respectively. The poor agreement between data and background simulations in the preselection category results from inadequate modelling of material near the beampipe in the forward region.

Cut	Data	ΣBkgd	e^+e^-	$\nu\bar{\nu}\gamma\gamma$	$\gamma\gamma$	$\ell^+\ell^-$	$e^+e^-f\bar{f}$	H40	H70
161 GeV									
$\nu\bar{\nu}\gamma\gamma$ presel.	85	19.18	16.65	0.98	1.30	0.04	0.21	0.65	0.70
$\theta_{\gamma 1}$	20	14.40	12.77	0.98	0.64	0.02	0.00	0.64	0.70
$\theta_{\gamma 2}$	6	7.14	5.86	0.98	0.29	0.01	0.00	0.63	0.69
$\mathcal{L}(\gamma\gamma)$	1	0.67	0.04	0.55	0.08	0.00	0.00	0.54	0.58
172 GeV									
$\nu\bar{\nu}\gamma\gamma$ presel.	62	16.74	13.70	0.93	1.15	0.03	0.93	0.62	0.72
$\theta_{\gamma 1}$	20	12.35	10.61	0.93	0.59	0.01	0.21	0.61	0.72
$\theta_{\gamma 2}$	10	6.17	5.00	0.93	0.23	0.01	0.00	0.60	0.71
$\mathcal{L}(\gamma\gamma)$	2	0.54	0.00	0.44	0.10	0.00	0.00	0.53	0.62

Table 3: Events remaining after cumulative cuts indicated for the missing energy channel. The row denoted "$\nu\bar{\nu}\gamma\gamma$ presel." refers to the combined general low-multiplicity selection and the precuts described in Section 4.4. The contributions from Bhabha scattering, $\nu\bar{\nu}\gamma\gamma$, $\gamma\gamma$, lepton pair ($\ell \equiv \mu, \tau$) production and $e^+e^-f\bar{f}$ final states determined from background simulations are shown. The simulation datasets have been normalized to 10.0 pb^{-1} for $\sqrt{s} = 161$ GeV, and to 10.3 pb^{-1} for $\sqrt{s} = 172$ GeV. Also shown is the acceptance for a Higgs signal for 40 and 70 GeV mass denoted as columns "H40" and "H70", respectively. The poor agreement between data and background simulations in the preselection category results from inadequate modelling of material near the beampipe in the forward region.

Channel	$\sqrt{s}$(GeV)	$M_{\gamma\gamma}$(GeV)	M_{recoil} (GeV)	$E_{\gamma 1}$ (GeV)	$\cos\theta_{\gamma 1}$	$E_{\gamma 2}$ (GeV)	$\cos\theta_{\gamma 2}$
$\nu\bar{\nu}$	172	44.9	93.1	48.7	0.90	18.0	-0.27
$q\bar{q}$	161	42.2	79.9	39.2	-0.04	27.0	-0.81
$\nu\bar{\nu}$	172	39.9	92.6	51.1	0.05	14.7	0.79
$q\bar{q}$	172	36.8	90.4	60.3	0.63	5.8	-0.31
$q\bar{q}$	161	24.9	72.1	54.5	0.66	11.8	0.63
$\nu\bar{\nu}$	161	15.8	106.9	32.4	0.58	13.4	0.10
$q\bar{q}$	161	12.1	85.6	53.1	0.60	5.1	-0.10

Table 4: Masses and energies of candidate events from the LEP-2 search, after all cuts except the one on di-photon mass. The events are ordered by di-photon mass.

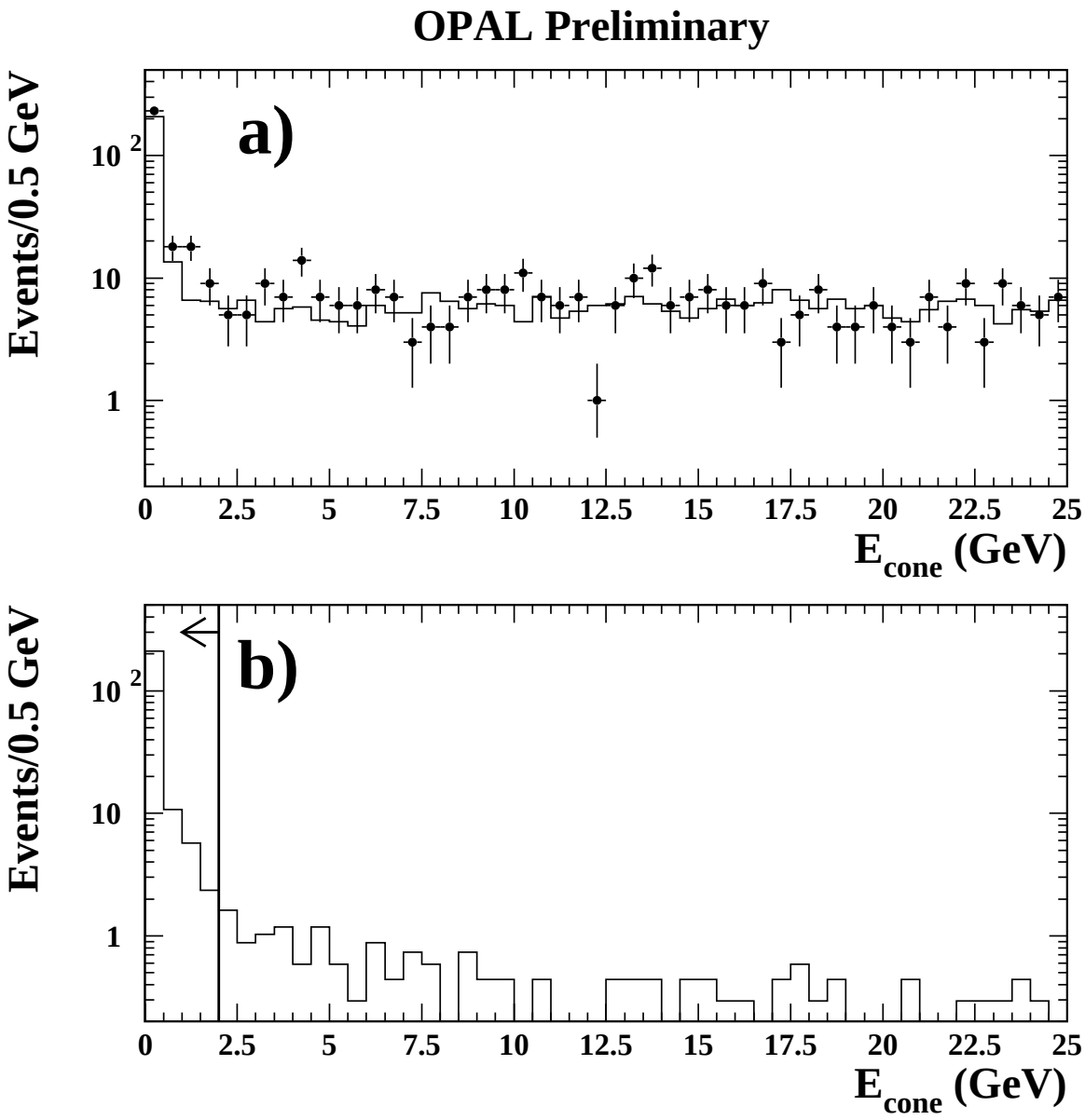

Figure 1: Distribution of charged-particle momentum and unassociated electromagnetic energy sum in 15° cones about the photon axes (for the hadron channel after multiplicity preselection). Figure a) shows 161 GeV data (points) and simulated background (histogram). Figure b) shows HZ production with Higgs mass = 40 GeV. The position of the cut is shown.

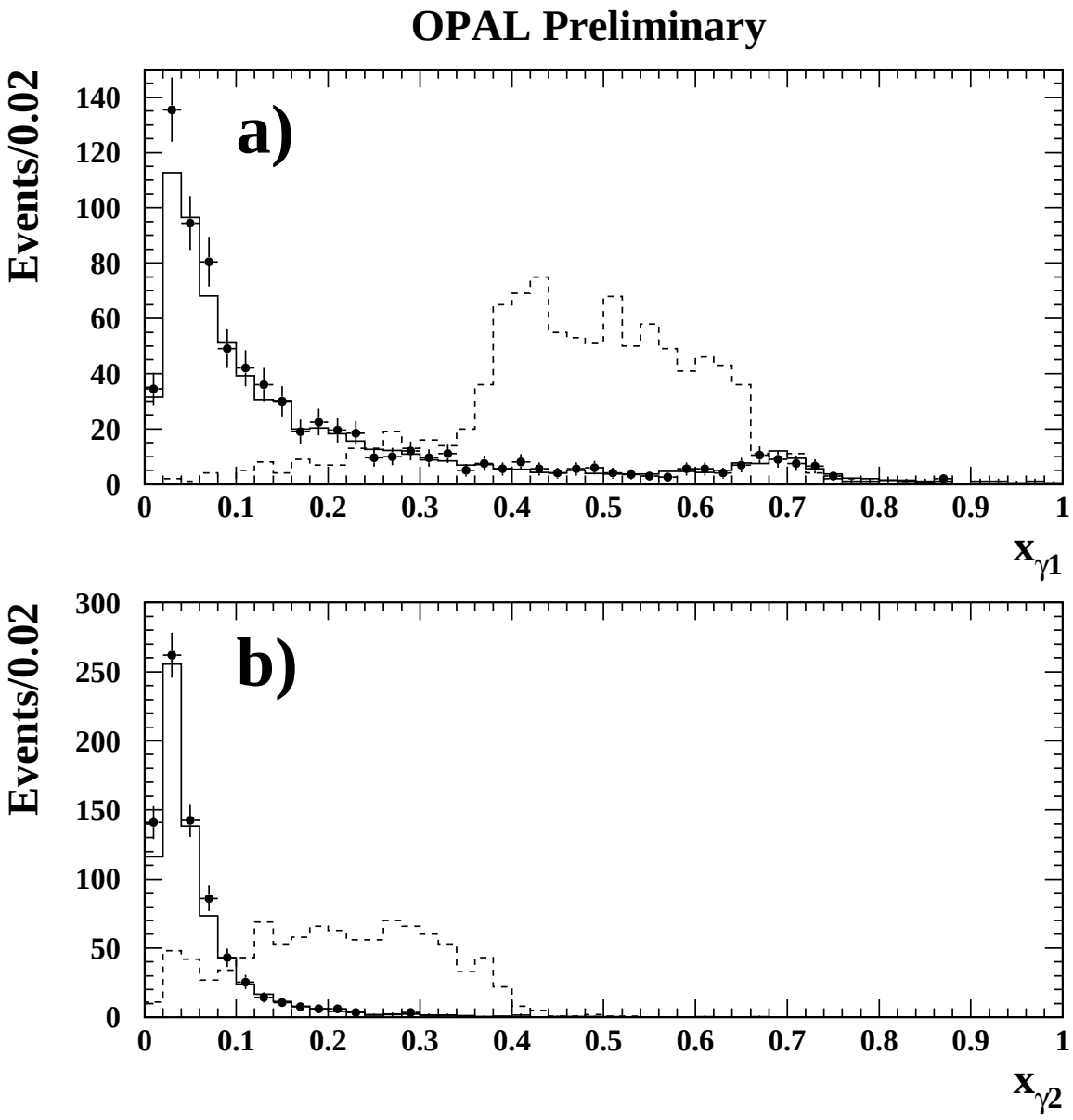

Figure 2: Distribution of $x_\gamma \equiv E_\gamma/E_{\rm beam}$ for the most energetic photon (a) and the second-most energetic photon (b) in the $\gamma\gamma$ + *hadrons* search, after the multiplicity preselection. Data from $\sqrt{s} = 161$ GeV are shown as points with error bars; background simulation is indicated by the histogram. The broken histogram shows H^0Z^0 production with $M_H = 40$ GeV.

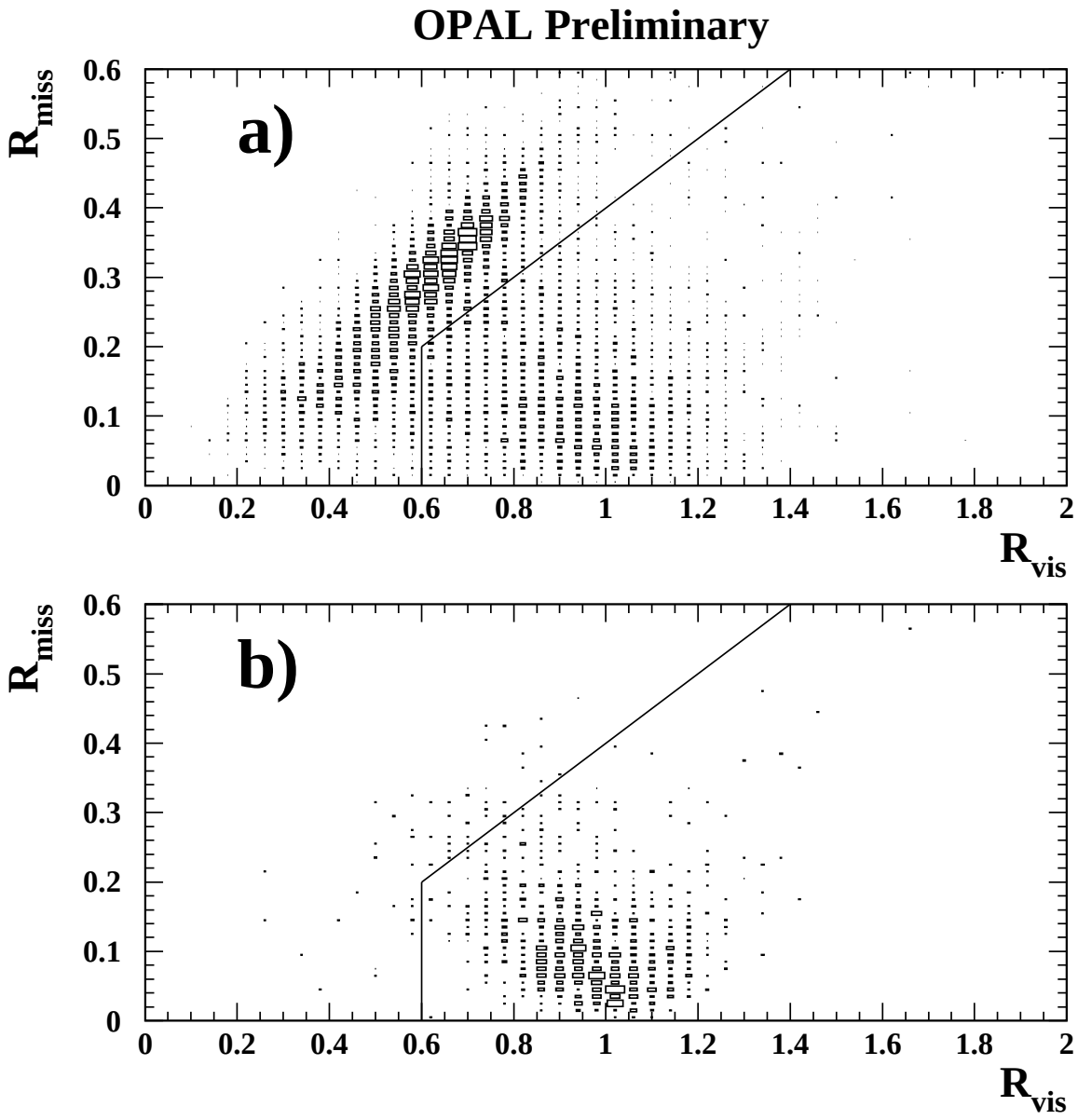

Figure 3: Distribution of fractional visible total energy versus fractional missing momentum for (a) simulation of $q\bar{q}$ events at $\sqrt{s} = 161$ GeV, and (b) simulation of Higgs events with $M_H = 40$ GeV. The cut used for the hadronic channel is shown by the solid line.

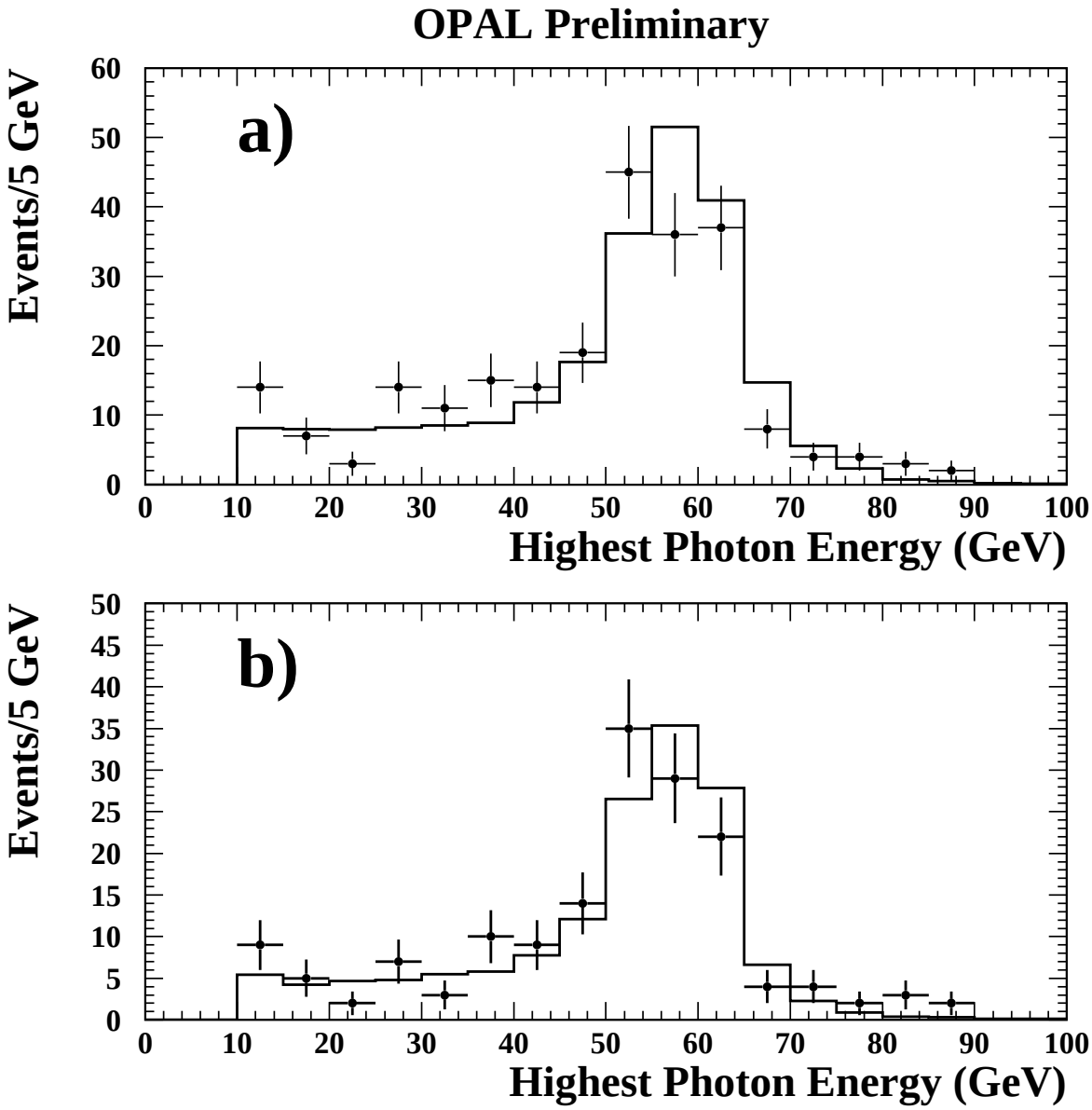

Figure 4: a) Distribution of highest photon energy for LEP-2 events ($\sqrt{s}$ = 161 and 172 GeV) passing the precuts and having at least one photon with $E_\gamma > 10.0$ GeV. Data are shown as points; background simulation is indicated by the histogram. The additional cut $|\cos(\theta_\gamma)| < 0.9$ is applied in b).

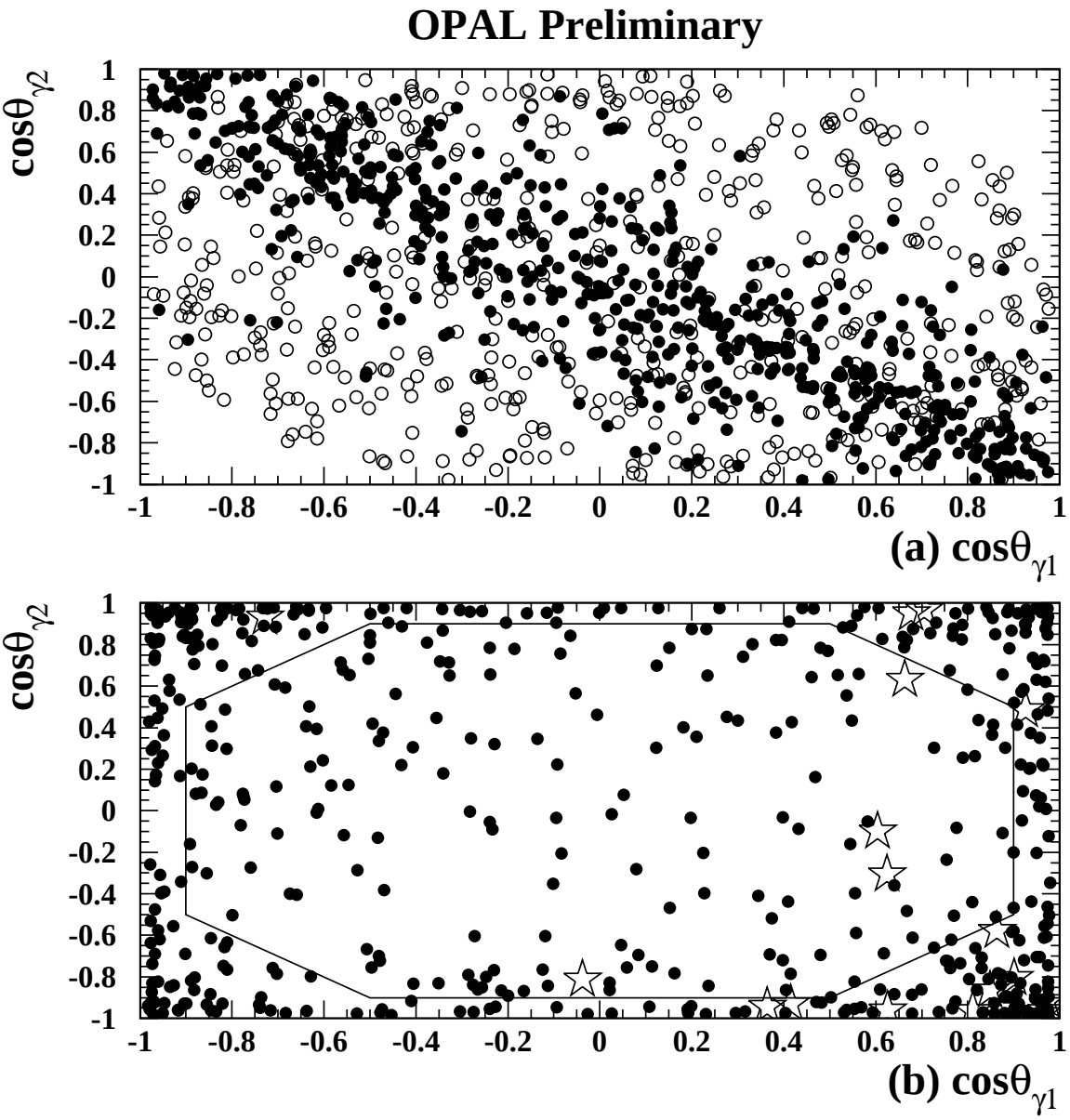

Figure 5: Distribution of $\cos\theta_{\gamma 1}$ and $\cos\theta_{\gamma 2}$ for simulation events of H^0Z^0 production at $\sqrt{s} =$ 161 GeV; the precuts have been applied. (a) shows simulated signal for $M_H = 40$ GeV (open circles) and $M_H = 70$ GeV (solid dots). (b) shows simulated $q\bar{q}$ events and the graphical cut boundary used in the hadronic channel. The data ($\sqrt{s} = 161$ and 172 GeV) are shown as open stars.

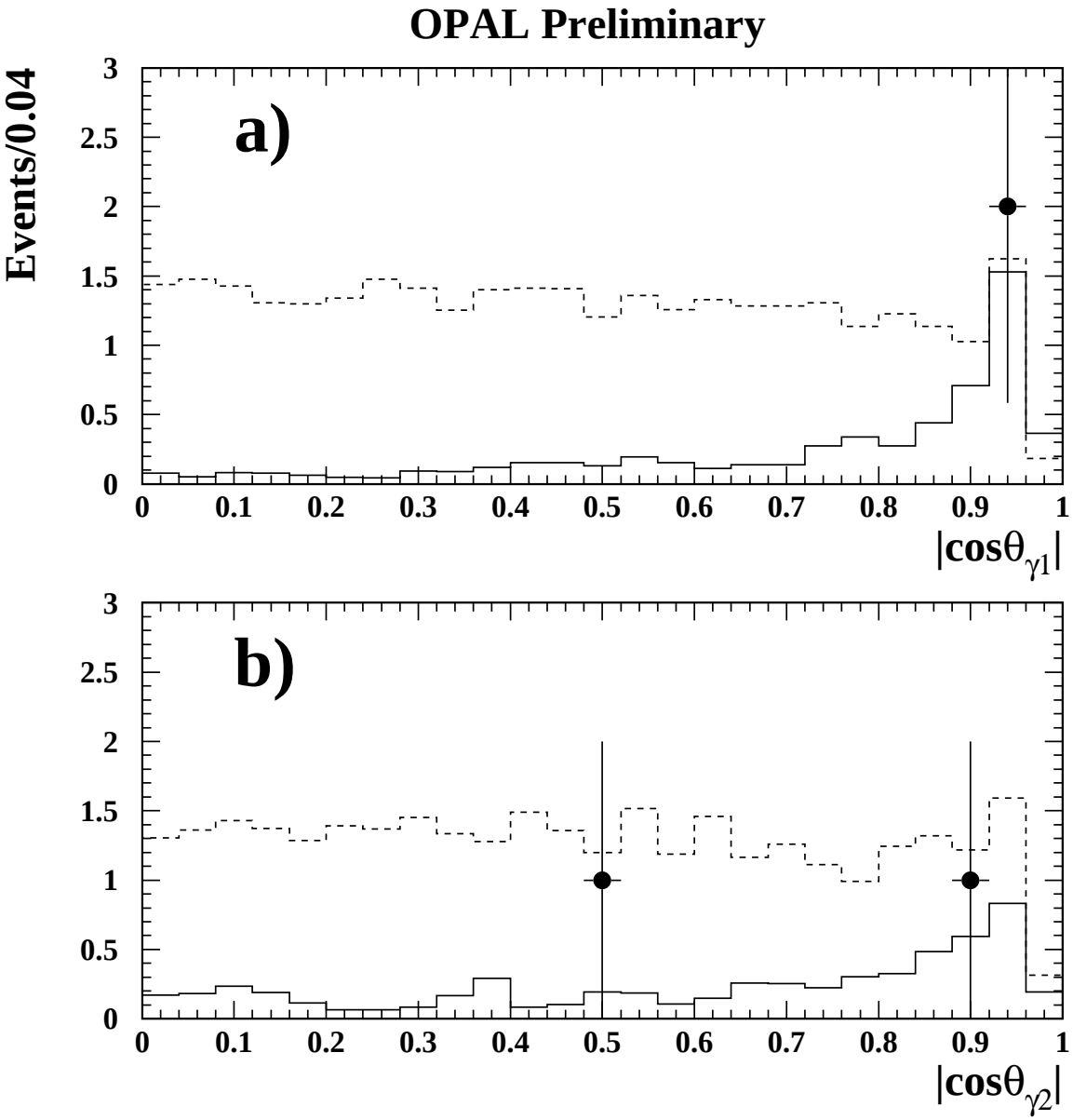

Figure 6: Distribution of photon polar angles for lepton channel LEP-2 event candidates, before the likelihood cut. The highest energy photon is shown in a); the lower energy photon is shown in b). Background simulation is indicated by the solid histogram. Distribution for a 70 GeV Higgs boson is indicated by the broken histogram.

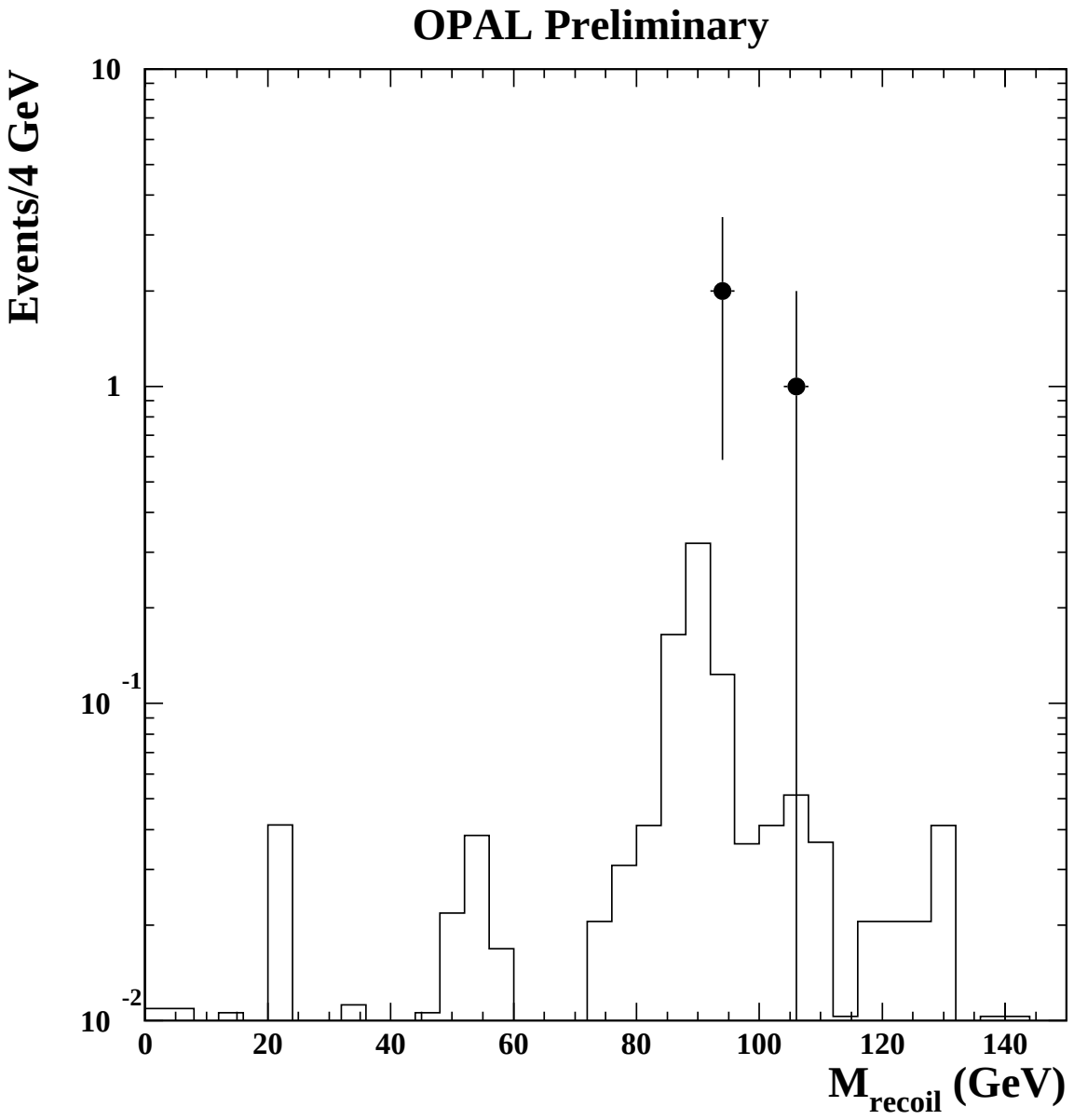

Figure 7: Recoil mass for event candidates in the missing energy channel, before the cut on $M_{\gamma\gamma}$. Background simulation is indicated by the solid histogram.

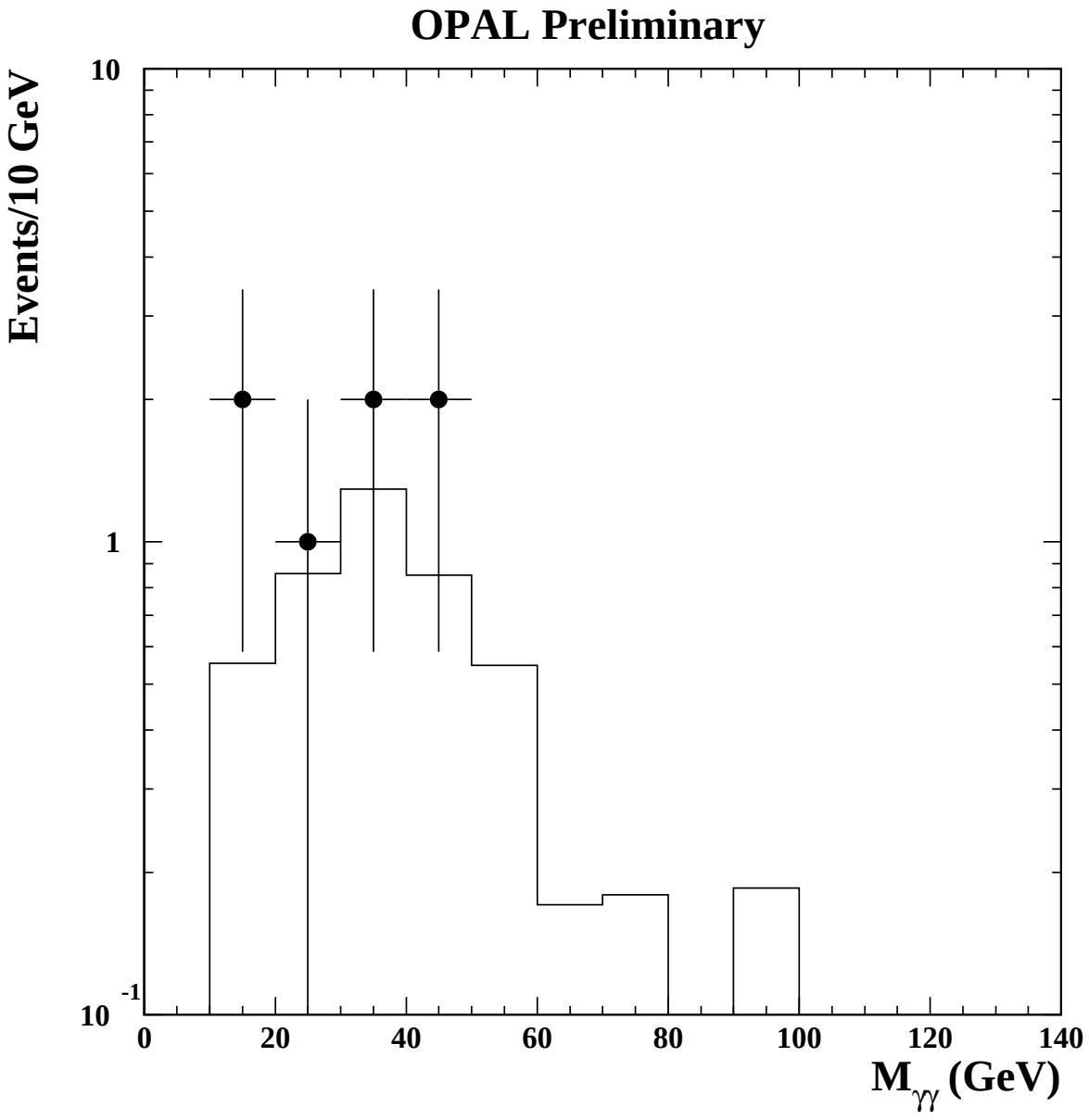

Figure 8: Distribution of mass of the 2 highest energy photons for events with $\sqrt{s} = 161$ and 172 GeV, after all cuts except the one on $M_{\gamma\gamma}$; all search channels are included. Data are shown as points with error bars; background simulation is shown as histogram.

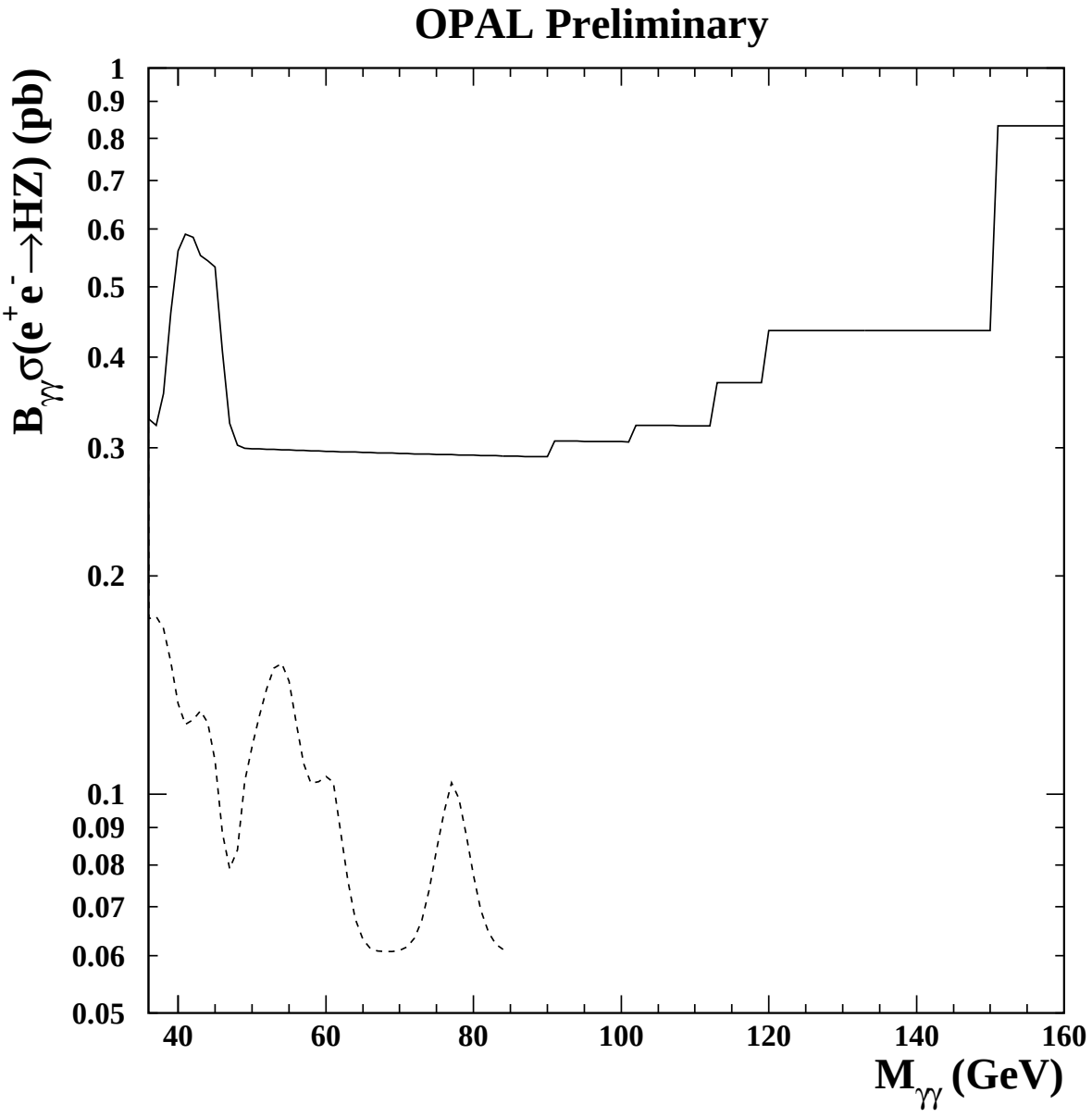

Figure 9: 95% Confidence Level Upper Limit on $B(H^0 \to \gamma\gamma) \times \sigma(e^+e^- \to H^0Z^0)$. Solid curve represents the LEP-2 limit; broken curve the LEP-1 limit.

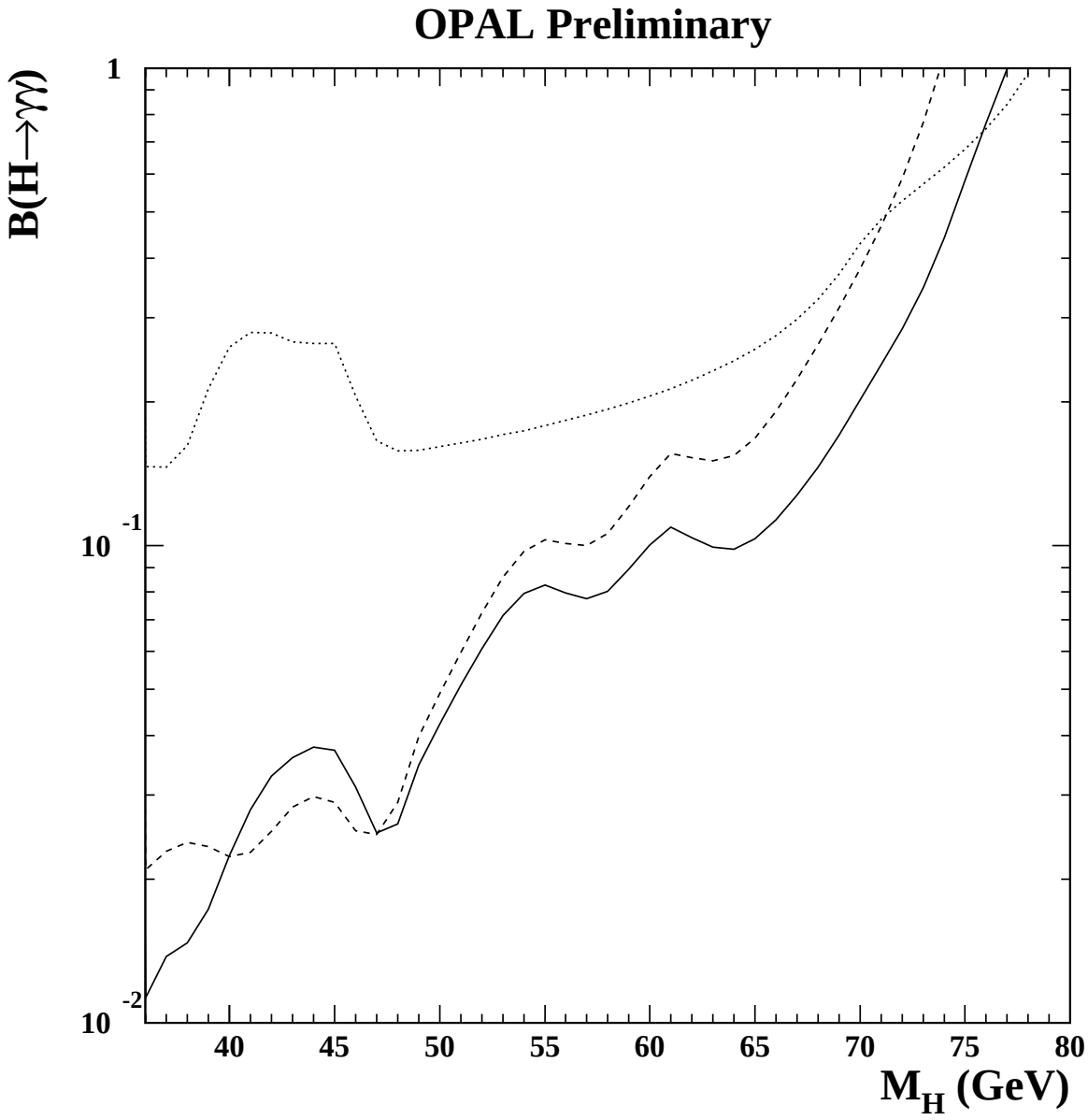

Figure 10: 95% Confidence Level Upper Limit on $B(H^0 \to \gamma\gamma)$ for Standard Model Higgs boson production using data from $\sqrt{s} = 91$ GeV (dashed line), 161 and 172 GeV (dotted line), and all data combined (solid line).

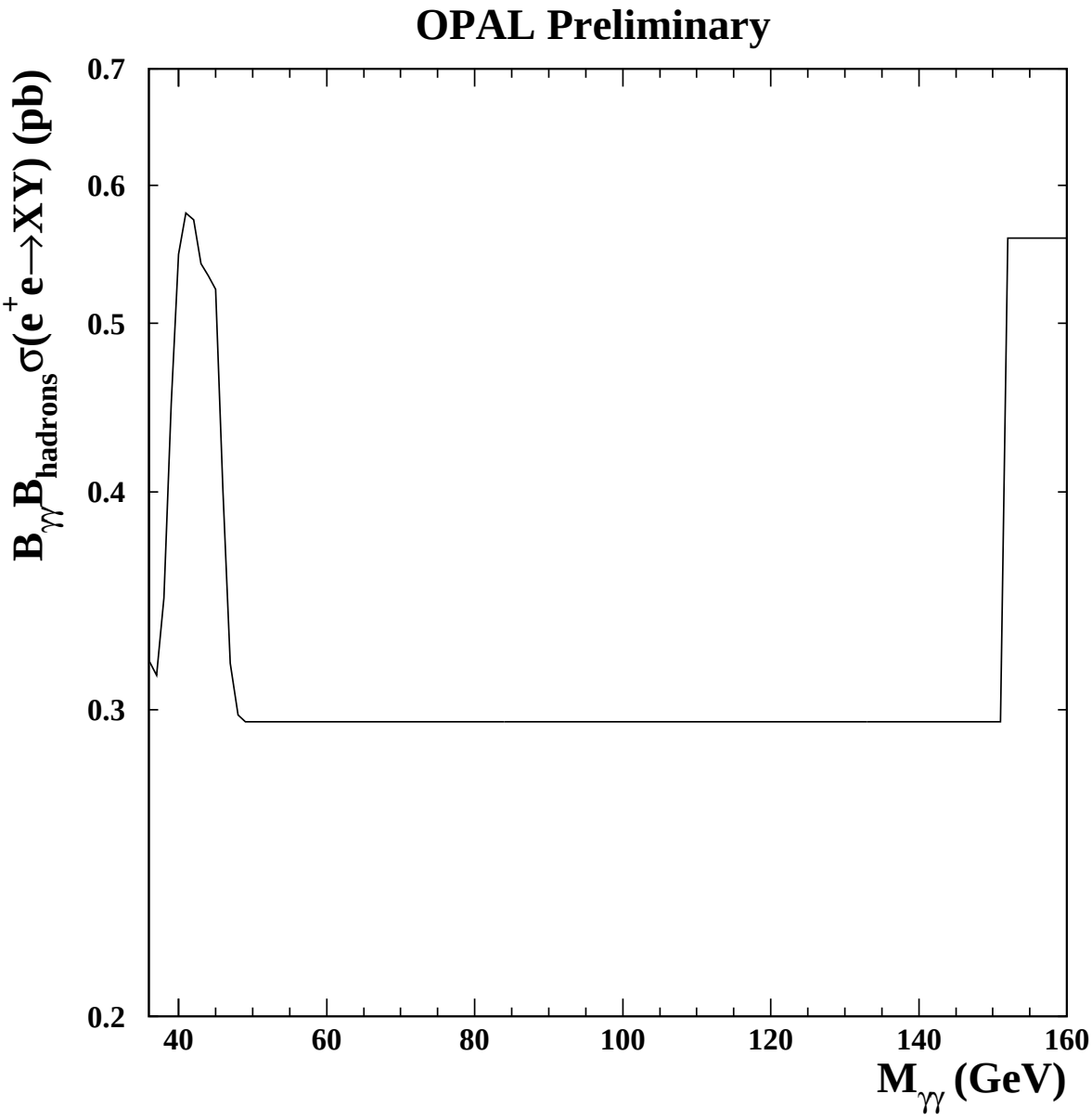

Figure 11: 95% Confidence Level Upper Limit on B(X $\to \gamma\gamma$)$\times$ B(Y $\to$ *hadrons*)$\times$ σ($e^+e^- \to$ XY), for scalar X and vector Y, using the hadronic channel analysis with data from LEP-2.